energies

MDPI

Article

Electrochemical Performance of Highly Conductive Nanocrystallized Glassy Alluaudite-Type Cathode Materials for NIBs

Maciej Nowagiel [1], Mateusz J. Samsel [1], Edvardas Kazakevicius [2], Aldona Zalewska [3], Algimantas Kežionis [2] and Tomasz K. Pietrzak [1,*]

[1] Faculty of Physics, Warsaw University of Technology, Koszykowa 75, PL-00-662 Warsaw, Poland; maciej.nowagiel.dokt@pw.edu.pl (M.N.); mateusz.samsel.stud@pw.edu.pl (M.J.S.)
[2] Faculty of Physics, Vilnius University, Saulėtekio 9, LT-10222 Vilnius, Lithuania; edvardas.kazakevicius@ff.vu.lt (E.K.); algimantas.kezionis@ff.vu.lt (A.K.)
[3] Faculty of Chemistry, Warsaw University of Technology, Noakowskiego 3, PL-00-664 Warsaw, Poland; aldona.zalewska@pw.edu.pl
* Correspondence: tomasz.pietrzak@pw.edu.pl

Abstract: Alluaudite-type materials are systematically attracting more attention as prospective cathode materials for sodium-ion batteries. It has been demonstrated that optimized thermal nanocrystallization of glassy analogs of various cathode materials may lead to a significant increase in their electrical conductivity. In this paper, three alluaudite-like glasses ($Na_2Fe_3(PO_4)_3$—FFF, $Na_2VFe_2(PO_4)_3$—VFF, and $Na_2VFeMn(PO_4)_3$—VFM) were synthesized and subjected to an optimized thermal nanocrystallization. This procedure resulted in nanostructured samples with increased electrical conductivity at room temperature: 5×10^{-7} S/cm (FFF), 7×10^{-5} S/cm (VFM), and 6×10^{-4} S/cm (VFF). The nanocrystalline microstructure was also evidenced by ultra-high-frequency impedance spectroscopy (up to 10 GHz) and proposed electrical equivalent circuits. Prototype electrochemical cells were assembled and characterized with voltage cutoffs of 1.5 and 4.5 V. The electrochemical performance was, however, modest. The gravimetric capacity varied between the studied materials, but did not exceed 35 mAh/g. Capacity retention after ca. 100 cycles was satisfactory. Further optimization of the residual-glass-to-nanocrystallite volume ratio would be desirable.

Keywords: glass ceramics; nanomaterials; cathode materials; nanocrystallization; alluaudite

Citation: Nowagiel, M.; Samsel, M.J.; Kazakevicius, E.; Zalewska, A.; Kežionis, A.; Pietrzak, T.K. Electrochemical Performance of Highly Conductive Nanocrystallized Glassy Alluaudite-Type Cathode Materials for NIBs. *Energies* **2022**, *15*, 2567. https://doi.org/10.3390/en15072567

Academic Editor: Nina V. Kosova

Received: 25 February 2022
Accepted: 25 March 2022
Published: 1 April 2022

1. Introduction

Renewable energy sources such as wind and solar are expected to play a significant role in the global energy transition [1]. However, they are also known as intermittent energy sources due to the fact that their operation depends on atmospheric conditions. Wind power stations produce energy when the wind blows, and solar plants do it only during the day. Thus, to meet the grid demand, it is necessary to store the surplus and utilize it during an undersupply period.

Li-ion batteries are widely used in portable electronics, electric vehicles, as well as energy storage systems that operate in one-day cycles. Their main advantages are an operating voltage of 3.2–4.0 V and an energy density of up to 250 Wh/kg (based on the weight of the entire cell) [2]. The cathodes in lithium cells have a high gravimetric capacity of 120–200 mAh/g and a lifetime of more than 1000 charge–discharge cycles [3]. Scientists struggle to find an inexpensive and widely available alternative to lithium. One of them can be sodium, which is also an alkaline metal. Sodium batteries usually have less capacity and have a lower operating voltage. Despite this, the energy density is still reasonably high, which makes them good candidates for sustainable and cost-efficient large-scale energy storage [4].

Alluaudite-type materials are proposed to become novel cathodes in sodium-ion batteries. Their theoretical gravimetric capacity reaches 170 mAh/g. Nevertheless, it is hard to obtain material with practical capacity close to the theoretical value. One of the reasons is the low electrical conductivity of the compounds.

The first reports on the possibility of applying alluaudites in reversible cells came from Richardson's 2003 work. He researched, among others, $NaFe_3(PO_4)_3$ and $Li_xNa_{2x}FeMn_2(PO_4)_3$ in lithium cells. The first one reached a gravimetric capacity of 30 mAh/g and the second one 125 mAh/g, while the theoretical value is 170 mAh/g. He also received $NaFe_3(PO_4)_3$ in amorphous form by rapid cooling of a molten mixture of reagents. The FTIR spectrum was characteristic of alluaudite [5].

In 2010, Trad investigated $NaMnFe_2(PO_4)_3$ obtained by solid-state reaction and the sol–gel method. The gravimetric capacity of the former was only 15 mAh/g. The material obtained by the sol–gel method was made up of smaller crystalline grains and had a porous structure, which led to an increase in capacity to 50 mAh/g. Difficulty in achieving the theoretical value (170 mAh/g) was mainly attributed to poor electronic conductivity [6].

Eight years later, Dwibedi made an attempt to improve the parameters of $NaMnFe_2(PO_4)_3$. Crystalline material with 100 nm grains coated with carbon reached a capacity of 60 mAh/g (at a C/20 current), but with a higher load, it dropped to 20 mAh/g (at a C current). The electrical conductivity was $\sigma(200\,^{\circ}C) = 1.2 \times 10^{-4}$ S/cm, $E_a = 0.163$ eV [7].

Essehli described $Na_{1.86}Fe_3(PO_4)_3$ with the capacity of 109 mAh/g while drawing low currents of 5 mA/g. After 100 cycles, 87% of the initial capacity remained still useful. At higher loads, the amount of charge that could be reversibly cycled dropped significantly (by over 30%). This was attributed to the low electrical conductivity [8].

Liu and Palmore investigated the effect of grinding $Na_{1.702}Fe_3(PO_4)_3$ material and coating it with carbon on sodium cell performance. It turned out that the best results were obtained when the material was ground to particles less than 200 nm and coated with carbon as well. The high capacity of 141 mAh/g (theoretical 160 mAh/g) was attributed to increased electrical conductivity, reduced resistance between the grains, and the better-organized surface of the coated material [9].

Walczak indicated that the $Na_{1.47}Fe_3(PO_4)_3$ obtained by the solid-state reaction method did not contain secondary crystalline phases, in contrast to $Na_2Fe_3(PO_4)_3$. Besides, she concluded that the cathode redox reactions were limited by the low Na^+ ion diffusion coefficient—ca. 5×10^{-14} cm^2/s [10].

A growing interest in alluaudites has caused an increasing number of publications in this topic. Many other groups put valuable efforts into research on alluaudite-type cathode materials for NIBs. A description of other works can be found, e.g., in [11].

To overcome the problem of the low electrical conductivity of various potential cathode materials, J.E. Garbarczyk, T.K. Pietrzak, and co-workers investigated the phenomenon of thermal nanocrystallization of amorphous analogues of cathode materials for lithium batteries (e.g., [12,13]). A correlation was observed between the increase in the electrical conductivity of the materials and changes in their microstructure. It was indicated that heating at an appropriate temperature resulted in the formation of small crystal grains of nanometric size embedded in the glassy matrix. It was concluded that such a microstructure creates favorable conditions for polaron hopping conductivity.

A similar approach was recently applied to alluaudite-type materials with a nominal composition of $Na_2Fe_3(PO_4)_3$, $Na_2VFe_2(PO_4)_3$, and $Na_2VFeMn(PO_4)_3$ [14]. It was shown that these compounds can be synthesized in a glassy form via the melt-quenching technique. Thermal nanocrystallization of these glasses usually resulted in an increase in the electrical conductivity of the material; however, the increase was often not satisfactory. Moreover, the low reproducibility of samples with a pure alluaudite phase was obscure. Therefore, in 2021, we focused on optimizing the synthesis conditions to strive for better phase purity and reproducibility, as well as the higher conductivity of alluaudite-type nanostructured glass ceramics. Three previously studied compositions were extensively investigated [15]. In particular, numerous factors influencing the final phase purity were carefully investigated,

and a set of optimized synthesis condition parameters was elaborated. Some differences occurred between materials of various compositions. Furthermore, numerous in situ electrical studies were carried out with a wide variety of the maximum temperature of the thermal nanocrystallization. As a result, nanomaterials with significantly improved electrical conductivity and high phase purity were synthesized.

For the purposes of this work, three alluaudite-like glasses with the compositions mentioned above were synthesized using optimized conditions, as described in [15]. Subsequently, they were subjected to a thermal nanocrystallization optimized procedure. Their impedance was studied at ultra-high frequencies. Eventually, prototype laboratory sodium cells were assembled, and their electrochemical properties were investigated.

2. Materials and Methods

The synthesis procedure was described in detail in [15]. In short, the following reagents were used: Na_2CO_3 (99.8%, Polish Chemicals), $FePO_4 \cdot 2H_2O$ (pure, Roth) or $FeC_2O_4 \cdot 2H_2O$ (99%, Aldrich), V_2O_5 (99.6%, Roth), $Mn(CH_3COO)_2 \cdot 4\,H_2O$ (99%, Aldrich), and $NH_4H_2PO_4$ (99%, Polish Chemicals).

$Na_2Fe_3(PO_4)_3$ (labeled as FFF) was synthesized using iron (II) oxalate as the Fe precursor. All reagents were mixed and homogenized in a mortar. The batches in porcelain crucibles were then placed in a chamber oven and presynthesized at 240 °C for 4 h. After that, the crucibles were put into an Argenta AFI-02 inductive furnace, preheated to 700 °C, heated to 1300 °C, and melted for 15 min. To ensure a non-oxidizing atmosphere, a double-crucible technique was used—the main crucibles were put into a larger one, filled with activated charcoal, and covered with a lid. At the end, the melt was poured onto a copper plate and immediately pressed with another one.

The procedure for the $Na_2Fe_2V(PO_4)_3$ (VFF) sample was similar. However, the batches were not presynthesized before melting and quenching was conducted between steel plates, and not copper ones.

$Na_2FeMnV(PO_4)_3$ (VFM), in turn, required iron (III) phosphate as the Fe precursor. The rest of the procedure was identical as that for the FFV sample.

The amorphousness of the as-synthesized samples and the structure of the nanocrystalline glass ceramics were investigated with X-ray diffractometry, using a Malvern Panalytical Empyrean diffractometer. The measurements were carried out in the 5–110° 2θ range at room temperature and using a copper lamp.

Electrical properties were studied by impedance spectroscopy (IS). The setup was based on a broadband impedance analyzer that performed measurements in the frequency range from 10 Hz to 7 GHz [16,17]. Pt electrodes were sputtered onto opposite faces of the solid samples in order to provide good electrical contacts. The impedance measurements were carried out on heating and cooling ramps in the temperature range from 25 °C to the optimal temperature determined for each composition (FFF—581 °C, VFF—628 °C, VFM—607 °C).

Active material for cathode preparation was synthesized as follows. Pristine glasses were heat treated in a tube furnace (Czylok) for 1 h at the temperature determined from the impedance measurements. Constant argon flow during the whole process was provided. The heating and cooling rates were set to 2 °C/min. The nanocrystalline glass ceramics were then ground in a mortar.

Each cathode layer had 3 constituents, which were mixed in the following proportions: active material—75%, conductive carbon black (Super P)—15%, polyvinylidene difluoride (PVDF) binder—10%. In the first step, only the active material and carbon black dried in a vacuum drier were mixed and then ball milled for 10 h at 100 rpm. Subsequently, a proper amount of binder was added, and a 1-methyl-2-pyrrolidinone solvent was used to prepare a slurry, which was put on a magnetic stirrer. After obtaining a smooth consistency, it was stirred further for at least 1 h. The cathode slurry was poured on aluminum foil and carefully but steadily spread by means of a doctor blade. The layer was preliminarily dried at ambient temperature in air for about 1 h. Then, it was placed in a vacuum drier at 55 °C overnight.

Electrochemical cells were assembled in Swagelok-type holders. A cathode disk was put into the cell in air. The rest of the process was performed in a glove box filled with argon. Glass microfiber separators were soaked with the electrolyte (1 M $NaClO_4$ solution in ethyl carbonate (EC) and propylene carbonate (PC) mixed at a 1:1 mass ratio), and metallic sodium (serving as an anode) was freshly rolled and cut. All components were put together and screwed sensitively in order not to damage the cathode layer, but to provide tightness and contact. When finished, the cells were additionally sealed with parafilm.

At the end, the cells were tested using the Arbin BT-2043 Battery Test System. The cycling procedure consisted of charge/discharge galvanostatic cycles with cut-off voltages of 1.5 V and 4.5 V. The cells were tested at various current rates, as follows: C/50 (1 cycle), C/20 (4 cycles), C/10 (20 cycles), C/5 (20 cycles), C/2 (20 cycles), C (20 cycles), C/10 (10 cycles). Current rates were calculated for the capacity considering only 2 active sodium ions per formula, i.e., 108 mAh/g.

3. Results

3.1. X-ray Diffractometry

The X-ray diffractometry (XRD) patterns of the as-synthesized glasses were typical for glassy materials and exhibited an amorphous halo at low angles and a lack of Braggs' reflexes. The patterns of the samples that were subjected to the optimized heat treatment are shown in Figure 1. A pattern of $Na_2Fe_2Mn(PO_4)_3$ alluaudite [18] (ICDD Card No. 04-012-0978) is given as a reference. The reflexes were noticeably broader than in the polycrystalline reference pattern. The average grain sizes were estimated using the Scherrer method. Firstly, the apparatus broadening of 0.08° was subtracted from the total experimental broadening. The calculated values of the grain size varied between samples and were equal to 50(4) mm, 46(3) mm, and 72(7) nm for the FFF, VFF, and VFM samples, respectively.

As expected, the XRD results proved that the nanocrystalline materials with superior phase purity were obtained as a result of their thermal treatment under the optimized conditions.

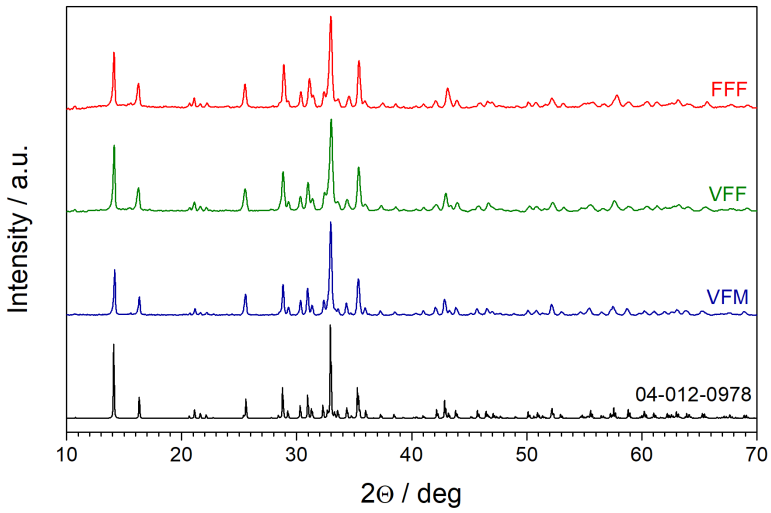

Figure 1. XRD patterns of nanocrystallized alluaudite-like glasses. A reference pattern of $Na_2Fe_2Mn(PO_4)_3$ alluaudite (ICDD Card No. 04-012-0978) is given at the bottom.

3.2. Impedance Spectroscopy

As already reported in [15], the electrical conductivity of the as-synthesized glasses was modest. The average values of σ_g at room temperature were as follows: $1.5(2) \times 10^{-8}$ S/cm, $2(1) \times 10^{-10}$ S/cm and $3.5(9) \times 10^{-11}$ S/cm for batches FFF, VFF, and VFM, respectively.

As a result of the optimized heat treatment, the conductivity of nanocrystalline materials was significantly higher (Figure 2). The temperature dependence of the conductivity followed the well-known Arrhenius formula, which is applicable to, among others, ionic, polaronic, and mixed conductors. The activation energy for the FFF sample decreased from

0.57 eV to 0.46 eV. The conductivity of the nanocrystalline sample was 5.6×10^{-7} S/cm. For the VFF sample, even greater enhancement was observed—E_a dropped from 0.71 eV to 0.21 eV and $\sigma_{nano}(25\,^{\circ}\mathrm{C})$ was 6×10^{-4} S/cm. The FMV sample had $E_a = 1.34$ eV in the high-temperature range and 0.88 eV at low temperatures, which decreased to 0.63 eV and 0.11 eV, respectively. The conductivity was as high as 6.7×10^{-5} S/cm. The increase of the conductivity (in comparison to the pristine glasses) was due to thermal nanocrystallization phenomenon [13], namely the appearance of nanocrystalline grains embedded in a residual glassy matrix. Such a microstructure was evidenced with a scanning electron microscopy in previous studies (Figure 7a–f in [15]). Highly disordered shells of the nanocrystals provided favorable conditions for electron hopping between aliovalent iron, vanadium, or manganese ions, e.g., Fe^{2+}/Fe^{3+}.

Analysis of the shape of the impedance figures revealed that all of the alluaudite samples—both glasses and nanomaterials—exhibited predominant electronic conductivity. In the case of the VFM sample, the high-temperature impedance spectra showed low-frequency spurs originating from ionic conductivity. This was the reason why the VFM samples exhibited different (higher) activation energies in the high-temperature range.

The complex impedance (represented in Nyquist plots) of the nanocrystalline materials, measured at room temperature, is shown in Figure 3a–c. In all cases, an equivalent circuit $(R_1P_1)(R_2P_2)(R_3P_3)$ was fit to the data. R represents the ohmic resistance, and P represents the constant phase element (CPE). At room temperature, the ionic conductivity was much lower than the electronic conductivity; thus, elements corresponding to the ionic conductivity were neglected in the equivalent circuits. The physical meaning of the (RP) parts is as follows: nanocrystalline interior (core), nanocrystalline boundary (grain), and residual glassy matrix in which the grains were embedded. A similar equivalent circuit was previously successfully proposed, e.g., for Bi_2O_3 nanocrystallites confined in a residual glassy matrix [19]. It is interesting to note that in the samples with high conductivity (VFF and VFM), one can observe at least one low-resistance semicircle in the high-frequency range. In this case, it can be attributed to the highly conductive shells of nanocrystalline grains [13].

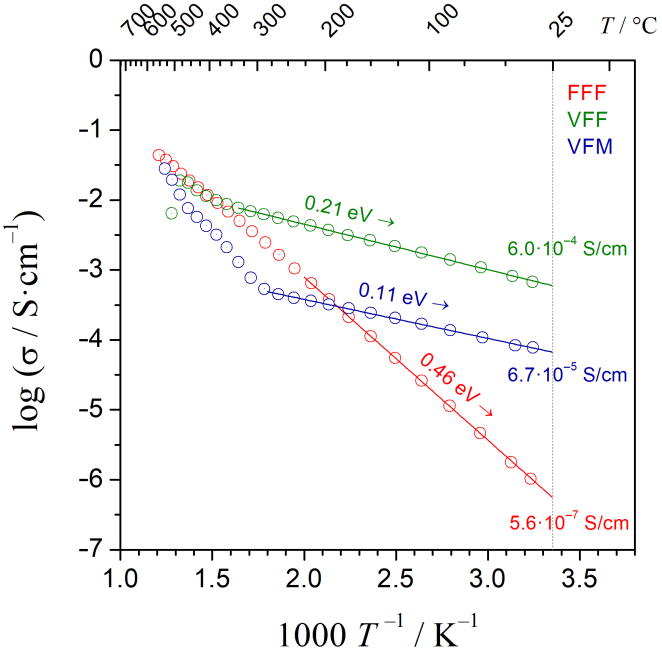

Figure 2. Electrical conductivity of nanocrystalline materials used for further cathode layer preparation. The values of the activation energy and conductivity at room temperature are given for each composition.

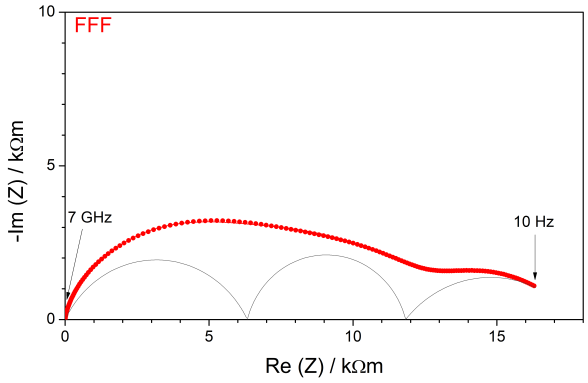

(**a**)

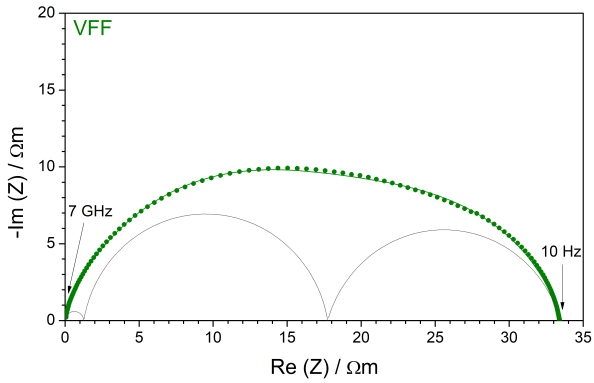

(**b**)

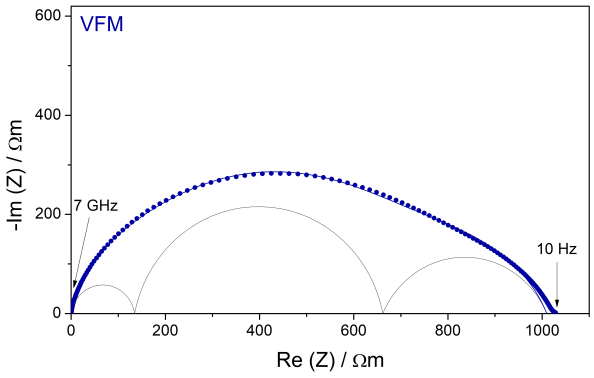

(**c**)

Figure 3. Impedance figures (Nyquist plots) of nanocrystalline materials measured at room temperature: FFF (**a**), VFF (**b**), and VFM (**c**). Total fits (colorful solid line) and partial fits of the (RP) elements (gray lines) are included in the plots.

3.3. Electrochemical Characterization

All cells were tested using the same procedure. Cycling was carried out at a constant current rate between voltages of 1.5 V and 4.5 V. Measurements began with one cycle at a C/50 current, followed by C/20, C/10, C/5, C/2, and C cycle series. The highest capacities in all materials were reached at low current rates. At the same time, the values were usually much lower than the theoretical capacity.

The cathode material FFF reached 22 mAh/g of charge capacity in the first cycle. Values for consecutive cycles were between 15 mAh/g and 3 mAh/g (Figure 4a). During the first cycle, the Coulomb efficiency was 66% and then gradually rose to over 98%

at higher currents. The capacities were low, but at the same time, the cycle life of the cathode was good. After 90 charge/discharge cycles, the capacity remained at a similar level (Figure 5a). The discharge curves for all currents were similar in shape (Figure 4b). In the C/50 curve, one can see a tiny plateau around 2.5 V, which vanished at higher currents. Both the charge and discharge capacities were very low—between 3 mAh/g and 15 mAh/g—and strongly depended on the current rate.

The cathode material VFF reached the capacity of 93 mAh/g during the first charge. Nonetheless, in consecutive cycles, the charge capacity was between 18 mAh/g and 3 mAh/g. The Coulomb efficiency gradually grew from as low as 20% in the first cycle to more than 80% in most of the following, up to 97% in the fastest cycles. This can mean that some irreversible processes occur during the first charge. The charge and discharge capacities significantly dropped at high current rates, but the cycle life was very good. The capacity after more than 90 cycles remained at the same level (Figure 5b). Figure 4c shows the charge curves at various current rates. Charge capacities reached modest values: 3 mAh/g to 18 mAh/g. They were similar to each other. There was no evident plateau, but one can distinguish some pitched steps—around 3.1 V, 3.7 V, and close to 4.5 V. Discharge curves (Figure 4d) revealed an inclined stretching step around 2.7 V.

The cathode material VFM did not show better electrochemical properties. The highest charge capacity of 40 mAh/g was reached in the second (C/20) cycle. In general, the capacities were between 2 mAh/g and 40 mAh/g and decreased significantly with increasing current rate. The Coulomb efficiency was lower for this material and ranged usually between 80% and 95% (Figure 5c). The lowest values (60–70%) were characteristic for cycles at the lowest current rates (C/50 and C/20). The Coulomb efficiency in the first (C/50) cycle was 107%; however, it was followed by the C/20 cycle with an efficiency of only 58%. It is distinctive for this material that the capacity gradually dropped in the first C/10 cycle series. Later on, however, the capacity was low, but remained at the same level within the next cycle series. After more than 80 cycles, the capacity remained at a similar level. The shape of all charge curves was similar—it was difficult to mark out any plateaus, as the curves were rather arc-like (Figure 4e). The discharge curves (Figure 4e) were step-like. One can distinguish stretched, inclined steps around 3.5 V, 2.7 V, and 2.25 V.

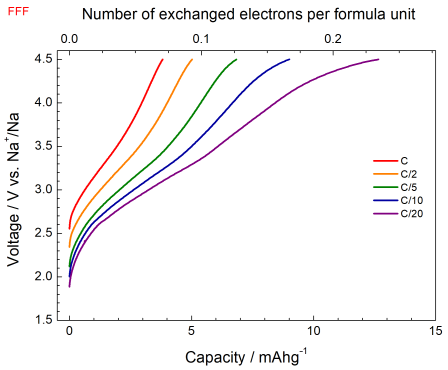

(**a**) FFF (charge)

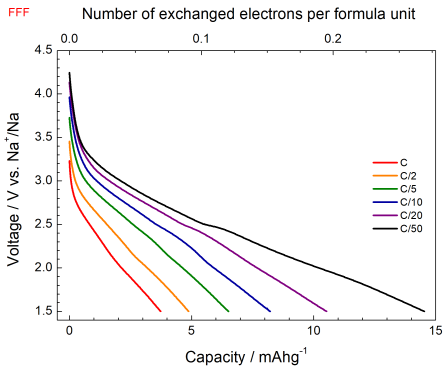

(**b**) FFF (discharge)

Figure 4. *Cont.*

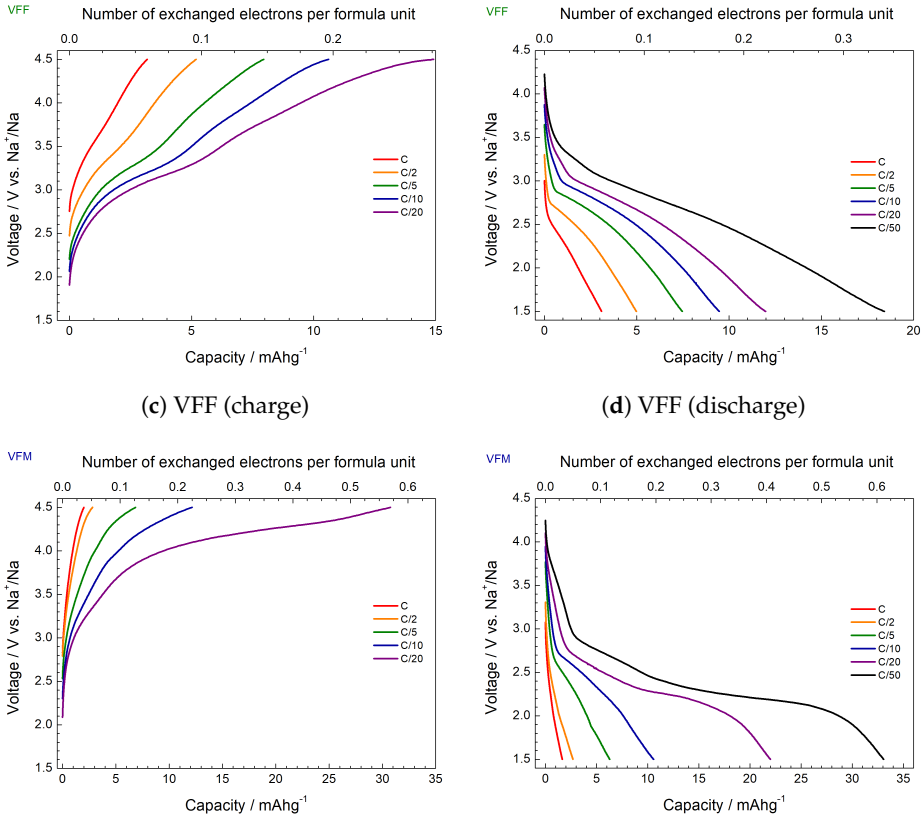

(**c**) VFF (charge) (**d**) VFF (discharge)

(**e**) VFM (charge) (**f**) VFM (discharge)

Figure 4. Typical charge and discharge curves for the FFF (**a**,**b**), VFF (**c**,**d**), and VFM (**e**,**f**) cathode materials taken at various current ranges from C/50 to C.

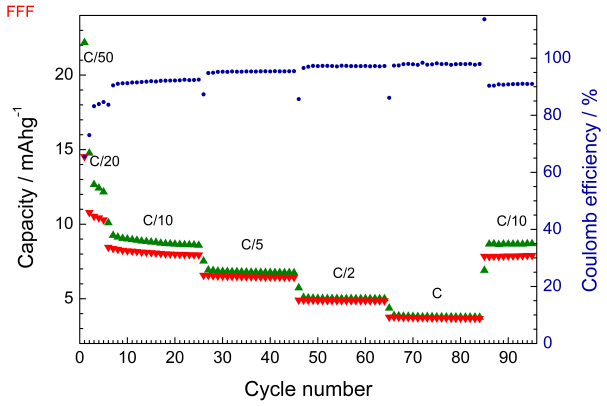

(**a**)

Figure 5. *Cont*.

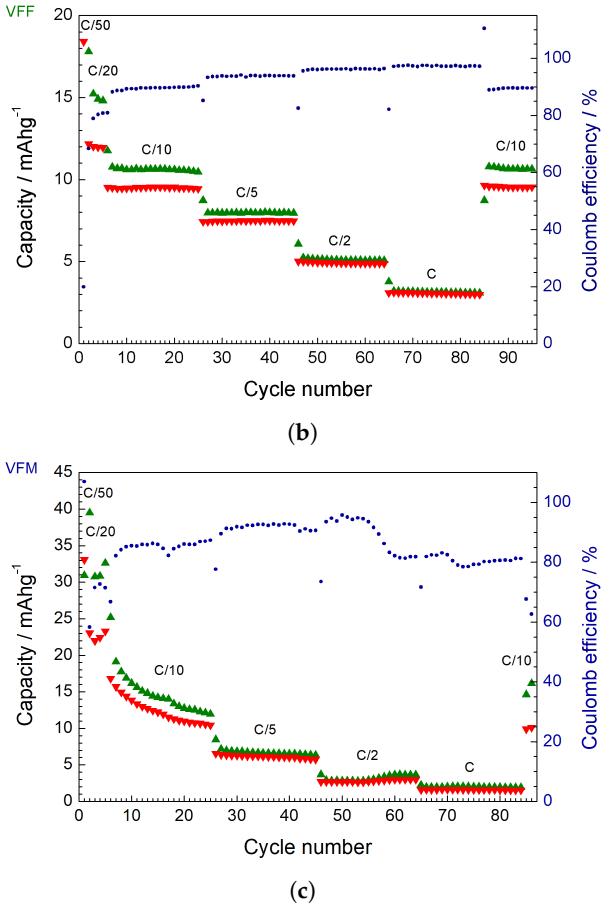

Figure 5. Cyclability and Coulombic efficiency of the studied cathode materials: FFF (**a**), VFF (**b**), and VFM (**c**). Charge (green "up" triangles) and discharge capacities (red "down" triangles) are compared to the Coulombic efficiency (blue dots) in consecutive cycles.

4. Conclusions

This work was a natural continuation of our recent study [15], where highly conductive nanocrystalline alluaudite-like materials were synthesized and their thermal, structural, and electrical properties were extensively studied. Here, we focused on the electrochemical performance of the active materials with optimized electrical conductivity.

Unfortunately, despite the high electrical conductivity and extended surfaces of the nanocrystalline grains, the electrochemical performance of the studied materials was modest. The highest reversible capacity did not exceed 35 mAh/g. Interestingly, the charge/discharge curves for nanocrystalline samples did not show standard plateaus. They were rather arc-like or had a stretched step-like shape. This is characteristic for nanostructured cathode materials, as shown, e.g., in the paper [20]. The most steps could be distinguished in the VFM material. This suggests the activity of a few redox couples, which may be due to the presence of three different transition metals.

It seems that at this point, the high electrical conductivity of the nanocrystalline materials did not result in an improvement of the electrochemical performance of the laboratory cells. Even though the electronic conductivity was significantly improved, the ionic conductivity probably remained at a modest level, what may be the reason for modest electrochemical performance. Nevertheless, in our opinion, further optimization in the preparation of cathode layers and assembling prototype cells could lead to better performance. In particular, the optimization of the nanocrystallite-to-residual-glassy-matrix ratio could be a factor influencing the performance, as well as some other parameters (e.g., milling time and speed, layer thickness, etc.). The quite good recent electrochemical

results of nanocrystalline olivine-like nanomaterials [21] gives strong motivation for further studies in this area.

Author Contributions: Conceptualization and funding acquisition, T.K.P.; supervision and methodology, A.Z., A.K. and T.K.P.; investigation, M.N., M.J.S. and E.K.; visualization, M.N. and T.K.P., writing—original draft preparation, M.N. and T.K.P. All authors have read and agreed to the published version of the manuscript.

Funding: This research was funded by *POB Energy* of Warsaw University of Technology within the Excellence Initiative: Research University (IDUB) program.

Institutional Review Board Statement: Not applicable.

Informed Consent Statement: Not applicable.

Data Availability Statement: Not applicable.

Conflicts of Interest: The authors declare no conflict of interest.

Abbreviations

The following abbreviations are used in this manuscript:

XRD	X-ray diffractometry
IS	Impedance spectroscopy

References

1. IRENA. *Global Energy Transformation: A Roadmap to 2050 (2019 Edition)*; International Renewable Energy Agency: Abu Dhabi, United Arab Emirates, 2019. Available online: https://www.irena.org/publications/2019/Apr/Global-energy-transformation-A-roadmap-to-2050-2019Edition (accessed on 22 February 2022).
2. Chmielewski, A.; Kupecki, J.; Szabłowski, Ł.; Fijałkowski, K.J.; Zawieska, J.; Bogdziński, K.; Kulik, O.; Adamczewski, T. *Currently Available and Future Methods of Energy Storage*; WWF Poland: Warsaw, Poland, 2020; ISBN 978-83-60757-56-7.
3. Nitta, N.; Wu, F.; Lee, J.T.; Yushin, G. Li-ion battery materials: Present and future. *Mater. Today* **2015**, *18*, 252–264. [CrossRef]
4. Slater, M.D.; Kim, D.; Lee, E.; Johnson, C.S. Sodium-Ion Batteries. *Adv. Funct. Mater.* **2013**, *23*, 947–958. [CrossRef]
5. Richardson, T.J. Phosphate-stabilized lithium intercalation compounds. *J. Power Sources* **2003**, *119–121*, 262–265 [CrossRef]
6. Trad, K.; Carlier, D.; Croguennec, L.; Wattiaux, A.; Amara, M.B.; Delmas, C. $NaMnFe_2(PO_4)_3$ Alluaudite Phase: Synthesis, Structure, and Electrochemical Properties As Positive Electrode in Lithium and Sodium Batteries. *Chem. Mater.* **2010**, *22*, 5554–5562. [CrossRef]
7. Dwibedi, D.; Jaschin, P.W.; Gond, R.; Barpanda, P. Revisiting the alluaudite $NaMnFe_2(PO_4)_3$ sodium insertion material: Structural, diffusional and electrochemical insights. *Electrochim. Acta* **2018**, *283*, 850–857. [CrossRef]
8. Essehli, R.; Yahia, H.B.; Maher, K.; Sougrati, M.T.; Abouimrane, A.; Park, J.-B.; Sun, Y.-K.; Al-Maadeed, M.A.; Belharouak, I. Unveiling the sodium intercalation properties in $Na_{1.86}\square_{0.14}Fe_3(PO_4)_3$. *J. Power Sources* **2016**, *324*, 657–664. [CrossRef]
9. Liu, D.; Palmore, G.T.R. Synthesis, Crystal Structure, and Electrochemical Properties of Alluaudite $Na_{1.702}Fe_3(PO_4)_3$ as a Sodium-Ion Battery Cathode. *Acs Sustain. Chem. Eng.* **2017**, *5*, 5766–5771. [CrossRef]
10. Walczak, K.; Kulka, A.; Molenda, J. Alluaudite-$Na_{1.47}Fe_3(PO_4)_3$: Structural and electrochemical properties of potential cathode material for Na-ion Batteries. *Solid State Sci.* **2019**, *87*, 21–26. [CrossRef]
11. Dwibedi, D.; Barpanda, P.; Yamada, A. Alluaudite Battery Cathodes. *Small Methods* **2020**, *4*, 2000051. [CrossRef]
12. Pietrzak, T.K.; Wasiucionek, M.; Michalski, P.P.; Kaleta, A.; Garbarczyk, J.E. Highly conductive cathode materials for Li-ion batteries prepared by thermal nanocrystallization of selected oxide glasses. *Mater. Sci. Eng. B* **2016**, *213*, 140–147. [CrossRef]
13. Pietrzak, T.K.; Wasiucionek, M.; Garbarczyk, J.E. Towards Higher Electric Conductivity and Wider Phase Stability Range via Nanostructured Glass-Ceramics Processing. *Nanomaterials* **2021**, *11*, 1321. [CrossRef] [PubMed]
14. Chamryga, A.E.; Nowagiel, M.; Pietrzak, T.K. Syntheses and nanocrystallization of Na_2O-M_2O_3-P_2O_5 alluaudite-like phosphate glasses (M = V, Fe, Mn). *J. Non-Cryst. Solids* **2019**, *526*, 119721. [CrossRef]
15. Nowagiel, M.; Samsel, M.J.; Pietrzak, T.K. Towards high phase purity of nanostructured alluaudite-type glass ceramics cathode materials for sodium ion batteries. *Materials* **2021**, *14*, 4997. [CrossRef] [PubMed]
16. Kežionis, A.; Kazlauskas, S. *High Temperature Ultrabroadband Impedance Spectrometer*; International Workshop on Impedance Spectroscopy: Chemnitz, Germany, 2013; pp. 32–33.
17. Kežionis, A.; Kazlauskas, S.; Petrulionis, D.; Orliukas, A.F. Broadband Method for the Determination of Small Sample's Electrical and Dielectric Properties at High Temperatures. *IEEE Trans. Microw. Theory Tech.* **2014**, *62*, 2456–2461. [CrossRef]
18. Hatert, F.; Rebbouh, L.; Hermann, R.P.; Fransolet, A.M.; Long, G.J.; Grandjean, F. Crystal chemistry of the hydrothermally synthesized $Na_2(Mn_{1-x}Fe_x^{2+})_2Fe^{3+}(PO_4)_3$ alluaudite-type solid solution. *Am. Mineral.* **2005**, *90*, 653–662. [CrossRef]

19. Pietrzak, T.K.; Garbarczyk, J.E.; Wasiucionek, M. Stabilization of the delta-Bi_2O_3-like structure down to room temperature by thermal nanocrystallization of bismuth oxide-based glasses. *Solid State Ion.* **2018**, *323*, 78–84. [CrossRef]
20. Gibot, P.; Casas-Cabanas, M.; Laffont, L.; Levasseur, S.; Carlach, P.; Hamelet, S.; Tarascon, J.M.; Masquelier, C. Room-temperature single-phase Li insertion/extraction in nanoscale $Li_{(x)}FePO_4$. *Nat. Mater.* **2008**, *7*, 741–747. [CrossRef] [PubMed]
21. Frąckiewicz, J.E.; Pietrzak, T.K.; Boczar, M.; Buchberger, D.A.; Wasiucionek, M.; Czerwiński, A.; Garbarczyk, J.E. Electrochemical properties of pristine and vanadium doped $LiFePO_4$ nanocrystallized glasses. *Energies* **2021**, *14*, 8042. [CrossRef]